Quantitative Morphometric Analysis of Oral Epithelial Dysplasia using Deep Learning-Based Nuclear Segmentation

Lucca S. P. Lacerda*, Marcela F. A. Ribeiro†, Martinho C. R. Horta†, Giovanna R. Souto†, Alexandre X. Falcão‡, Gustavo K. Rohde§, Zenilton K. G. Patrocínio Jr* and Silvio Jamil F. Guimarães*
*Laboratory of Image and Multimedia Data Science (IMScience)
Pontifical Catholic University of Minas Gerais,Belo Horizonte, Brazil
†Institute of Biological Science and Health
Pontifical Catholic University of Minas Gerais, Belo Horizonte, Brazil
‡Institute of Computing
Unicamp, Campinas, Sao Paulo, Brazil
§ Imaging and Data Science Lab
University of Virginia, Charlottesville, VA, USA
Email: lsplacerda@sga.pucminas.br, zenilton@pucminas.br, gustavo@virginia.edu, abrahao.marcela@hotmail.com, martinhohorta@pucminas.br, grsouto@hotmail.com, alexandre.falcao@gmail.com, sjamil@pucminas.br

***Abstract*—Oral Epithelial Dysplasia (OED) is a histopathological diagnosis for potentially malignant lesions with a variable risk of malignant transformation. The conventional grading of OED relies on morphological assessment, a process known for significant inter-observer variability, which limits its prognostic reliability. This study leverages computational pathology to address this challenge by employing a deep learning-based tool, Cellpose, for the precise segmentation of epithelial cell nuclei. The objective was to facilitate the objective extraction and analysis of key nuclear morphometric features, such as area, perimeter, and compactness, from digitized histological images of OED. We utilized 30 H&E-stained images from a spectrum of diagnostic categories, including normal oral mucosa, dysplasias of varying grades, and oral squamous cell carcinoma (OSCC). The results demonstrated that quantitative features, particularly the variance in nuclear area (anisonucleosis), serve as a robust differentiator between diagnostic grades, with the most significant changes observed in OSCC. By providing a reproducible and quantitative framework, this deep learning-driven approach represents a significant step towards a standardized diagnostic support system for OED, with future potential for accurately predicting malignant transformation risk.**

Keywords: Oral Epithelial Dysplasia, Image Segmentation, Computational Pathology, Nuclear Morphometry, Malignant Transformation, Artificial Intelligence.

I. Introduction

Oral cancer, predominantly Oral Squamous Cell Carcinoma (OSCC), remains a significant global health challenge with high morbidity and mortality rates, largely due to late-stage diagnosis [1], [2]. The detection and management of Oral Potentially Malignant Disorders (OPMDs) are paramount to improving patient outcomes. Among these, Oral Epithelial Dysplasia (OED) is the most critical histopathological finding, representing a spectrum of architectural and cytological changes that indicate an increased risk of progression to invasive carcinoma [3]. The current standard for diagnosing and grading OED is based on the microscopic evaluation of Hematoxylin and Eosin (H&E) stained tissue sections, as outlined by the World Health Organization (WHO) classification system [4]. This system categorizes OED into grades based on features such as nuclear pleomorphism (variation in shape) and anisonucleosis (variation in size) [5].

Despite its widespread use, this grading system is fraught with limitations, most notably its high degree of inter- and intra-observer subjectivity [6], [7]. This variability can lead to inconsistent clinical management and fails to reliably predict which lesions will progress to cancer [8]. To overcome these challenges, the field of computational pathology has emerged, leveraging digital image analysis and Artificial Intelligence (AI) to extract objective, quantitative data from histological slides [9]. A critical first step in this pipeline is accurate image segmentation. For OED analysis, the precise delineation of individual epithelial cell nuclei is essential for extracting the morphometric features that define dysplasia [10].

This study utilizes **Cellpose**, a deep learning-based segmentation tool, to automate the delineation of nuclei in complex histological images of OED. The primary objective of this research was to employ this automated method to extract and analyze key morphometric features across the spectrum of OED and OSCC, thereby establishing a quantitative and reproducible framework for assessing dysplastic changes. This work aims to lay the groundwork for a more objective and prognostically powerful approach to managing OED. The main contributions of this work are twofold: (i) nuclei segmentation by using a deep learning-based segmentation tool; and (ii) the study of quantitative morphometric of oral epithelial dysplasia from the segmented nuclei.

This paper is organized as follows. In Section II, we describe the materials and methods used for case selection, image acquisition, and our computational pipeline for nuclear segmentation and analysis. Section III presents the quantitative results of our morphometric analysis. In Section IV, we discuss the implications of these findings and the limitations of the study. Finally, Section V concludes the paper.

II. Materials and Methods

A. Case Selection and Histological Preparation

This study was conducted using archived, formalin-fixed, paraffin-embedded (FFPE) tissue blocks from five distinct cases previously diagnosed with OED, obtained with ethical approval from the institutional review board. For each case, 4-μm thick sections were cut and stained with Hematoxylin and Eosin (H&E) according to standard laboratory protocols.

B. Digital Image Acquisition

The H&E-stained glass slides were digitized to create the dataset. A total of 30 high-resolution digital images were captured from the epithelial layers across the lesions. The images were acquired using an Olympus BX51 optical microscope (Olympus Corporation, Tokyo, Japan). All images were captured under 400x magnification (40x objective lens) to ensure sufficient detail for nuclear analysis and saved in an uncompressed TIFF format.

C. Nuclear Segmentation and Expert-Guided Cell Pruning

The segmentation of epithelial nuclei was performed using Cellpose, a state-of-the-art, deep learning-based segmentation algorithm [11]. Cellpose is a generalist tool whose architecture is based on a U-Net model. Instead of predicting class labels for pixels, it computes a vector gradient field for each pixel, pointing towards the center of the cell. This method is highly effective at separating touching and overlapping nuclei, a common challenge in histological images of dysplastic tissue. We utilized the pre-trained 'cyto2' model, and the automated segmentation results were subjected to a quality control process where an evaluator performed manual corrections to fix any segmentation errors, such as inaccurate boundaries.

Following this initial segmentation, a crucial expert-guided cell pruning phase was conducted to ensure that only diagnostically relevant nuclei were included in the final morphometric analysis. Two specialists in oral pathology independently reviewed the segmented masks overlaid on the original H&E images. The selection was based on strict criteria: only epithelial cell nuclei clearly belonging to the basal and parabasal layers were retained. Nuclei from inflammatory infiltrates, stromal cells, those exhibiting significant artifacts (e.g., being partially out of the image frame or having poor staining), or those from superficial, fully differentiated epithelial layers were explicitly excluded from the dataset. This expert-driven pruning step was critical for refining the dataset to the cells of interest, thereby enhancing the clinical relevance of the subsequent quantitative analysis.

D. Quantitative Morphometric Feature Extraction and Analysis

Subsequent to the segmentation and expert-driven cell pruning, the refined set of selected nuclei was subjected to a quantitative morphometric analysis pipeline. A pixel-to-micrometer calibration factor, derived from the image acquisition settings, was applied to ensure all measurements were in standardized metric units. Three primary features were extracted. The **nuclear area** was calculated as the total number of pixels within the segmented boundary (μm²). The **perimeter** was computed as the length of the nuclear contour (μm). To quantify variations in nuclear shape, a **compactness** descriptor was calculated using the formula $C = \frac{4\pi \times \text{Area}}{\text{Perimeter}^2}$. A value of 1.0 indicates a perfect circle, with lower values signifying increasing shape irregularity. These features serve as quantitative proxies for anisonucleosis (variation in size) and nuclear pleomorphism (variation in shape).

The complete feature set was stratified into six diagnostic categories: Normal Mucosa, Mild Dysplasia, Moderate Dysplasia, Severe Dysplasia, Carcinoma in Situ, and OSCC. Descriptive statistics (mean and standard deviation) were computed for each feature within every category. The complete workflow, from sample preparation to quantitative analysis, is illustrated in Figure 2.

III. Results

A. Overview of Segmentation

The Cellpose segmentation pipeline was successfully applied to the entire dataset. A total of **10,106** epithelial nuclei were accurately segmented and analyzed across the six diagnostic categories. The number of cells analyzed per category is detailed in Table I. Figure 4 provides a visual example of the segmentation method's output, showing the precise delineation of nuclear boundaries.

B. Quantitative Morphometric Analysis

The extracted morphometric data revealed distinct trends across the diagnostic spectrum. The summary statistics, presented in Table I, show a progressive increase in the variability of nuclear area—a quantitative measure of **anisonucleosis**. The standard deviation (SD) of the area is markedly higher in moderate dysplasia, severe dysplasia, and especially in OSCC, which also exhibited the largest mean nuclear area.

To provide a more detailed view beyond summary statistics, the complete distributions of the key morphometric features were visualized across all diagnostic categories, as shown in Figure 3. This global quintile analysis reveals a distinct trend in **Area** and **Perimeter**. For Normal Mucosa (Fig. 3a), the cell population is heavily concentrated in the lowest quintiles (Quintile 0 and 1). As the lesion grade advances towards Severe Dysplasia and OSCC (Fig. 3d-f), a marked and progressive shift occurs, with a significantly larger proportion of nuclei populating the highest quintiles (Quintile 3 and 4). This visualization strongly corroborates the statistical findings of anisonucleosis presented in Table I, offering a more granular understanding of the underlying distributional changes. In

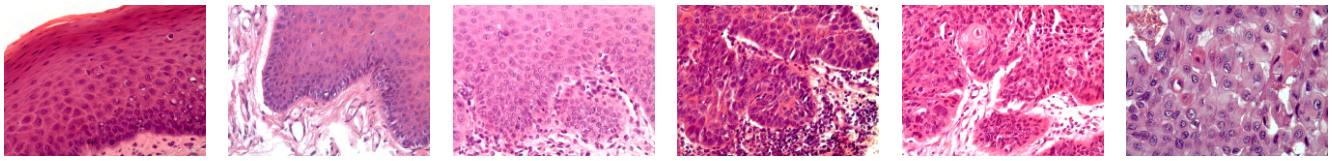

(a) Normal Mucosa (b) Mild Dysplasia (c) Moderate Dysplasia (d) Severe Dysplasia (e) Carcinoma in Situ (f) OSCC

Fig. 1. Visual comparison of nuclear morphology across the diagnostic spectrum. Representative image patches are shown for (a) Normal Mucosa, (b) Mild Dysplasia, (c) Moderate Dysplasia, (d) Severe Dysplasia, (e) Carcinoma in Situ, and (f) OSCC. A progressive increase in nuclear size, density, and shape irregularity (pleomorphism and anisonucleosis) is qualitatively evident, corresponding to the quantitative data in Table I and Figure 3.

TABLE I
SUMMARY OF NUCLEAR MORPHOMETRIC DATA ACROSS DIAGNOSTIC CATEGORIES

Diagnostic Category	**Number of Nuclei**	**Mean Area (μm^2) $\pm$ SD**	**Mean Perimeter (μm) $\pm$ SD**	**Mean Compactness $\pm$ SD**
Normal Mucosa	1470	1481.37 $\pm$ 838.40	147.69 $\pm$ 49.08	0.79 $\pm$ 0.27
Mild Dysplasia	2072	1149.21 $\pm$ 617.99	128.36 $\pm$ 39.91	0.82 $\pm$ 0.27
Moderate Dysplasia	1996	1913.91 $\pm$ 1169.44	160.53 $\pm$ 58.98	0.82 $\pm$ 0.27
Severe Dysplasia	1523	1765.95 $\pm$ 1050.72	156.72 $\pm$ 59.60	0.82 $\pm$ 0.38
Carcinoma in Situ	2349	1366.67 $\pm$ 994.70	137.65 $\pm$ 57.44	0.82 $\pm$ 0.34
OSCC	696	2378.48 $\pm$ 1416.19	182.99 $\pm$ 64.25	0.81 $\pm$ 0.20

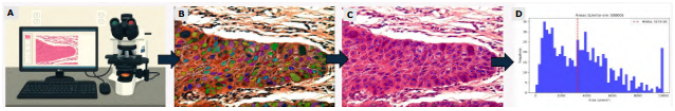

Fig. 2. Overview of the computational pipeline. The process begins with image acquisition from H&E slides, followed by automated nuclear segmentation using Cellpose. An expert-guided pruning step is then performed to select relevant cells before the final extraction of morphometric features and quantitative analysis.

contrast, the distribution for **Compactness** remains relatively consistent across all categories, reinforcing the observation that nuclear size variation was the most significant morphometric differentiator in this cohort.

C. Visualization of Segmentation

Figure 4 provides a representative example of the segmentation output from Cellpose. The accurate delineation of individual nuclear boundaries allows for a direct visual appreciation of the morphometric data presented in Table I, clearly illustrating the significant variation in nuclear size within the dysplastic and carcinomatous epithelium.

IV. Discussion

The histopathological diagnosis of OED is a cornerstone of oral cancer prevention, yet it is hampered by the subjective nature of morphological interpretation. This study demonstrates the utility of a deep learning-based approach using Cellpose for automated nuclear segmentation and objective morphometric analysis. Our findings confirm that this computational method can translate subjective cytological features into precise, quantitative measurements, thereby addressing the critical issue of diagnostic variability.

The strength of using a tool like Cellpose lies in its robust, deep learning-based architecture. While traditional automated segmentation methods often struggle with complexities like cellular overlapping and faint nuclear boundaries [12], Cellpose utilizes a state-of-the-art model that computes vector fields to precisely separate even densely packed nuclei. This automated method provides a highly reproducible and accurate foundation for quantitative analysis, reducing the subjectivity and extensive manual effort associated with older techniques.

The data presented in Table I illustrates how this quantitative approach can reveal important biological trends. The most striking finding was the marked increase in the standard deviation of nuclear area, which quantitatively represents anisonucleosis. This feature was a powerful differentiator, especially for identifying OSCC, which showed the highest degree of size variation. This transition from qualitative descriptors (“mild” or “moderate” anisonucleosis) to quantitative metrics is fundamental for building standardized diagnostic models suitable for machine learning applications [13], [14].

Interestingly, the mean compactness, our proxy for pleomorphism, did not show significant variation across the diagnostic groups. This suggests that for this dataset, nuclear size heterogeneity (anisonucleosis) is a more dominant and discriminative feature of malignant progression than nuclear shape irregularity. The accurate delineation of nuclei by Cellpose is the foundation upon which more complex analyses, such as chromatin texture analysis or spatial distribution patterns, can be built to further enhance predictive models [15].

A. Limitations and Future Directions

While promising, this study has limitations. The sample size was small, consisting of 30 images from five OED lesions1. A larger, multi-center cohort is required to establish the generalizability of our findings. Second, this study focused on the validation of the computational approach itself, not on the correlation of its output with long-term clinical outcomes.

The logical next step is to apply the validated Cellpose pipeline to a large cohort of OED cases with known clinical follow-up. By extracting morphometric and other features

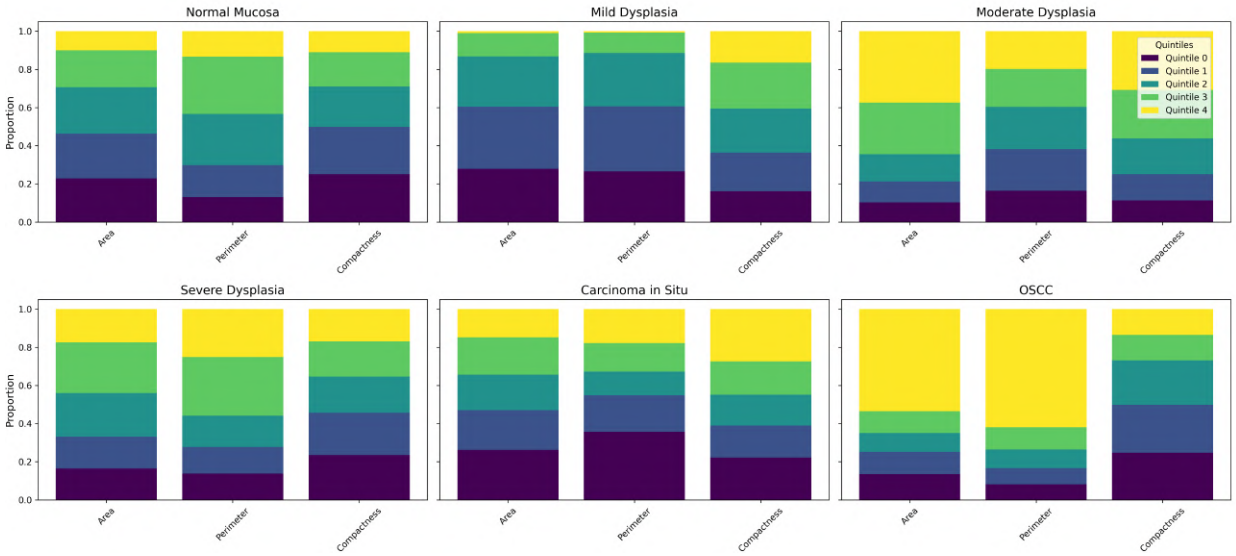

Fig. 3. Distribution of nuclear morphometric features across the diagnostic categories based on a global quintile analysis. For each feature (Area, Perimeter, Compactness), the stacked bars show the proportion of nuclei from that category falling into five global quintiles. Quintile 0 (dark purple) represents the smallest 20% of all nuclei in the entire dataset, while Quintile 4 (yellow) represents the largest 20%. A clear progressive shift towards higher quintiles is evident for Area and Perimeter as lesions advance from Normal Mucosa (a) to OSCC (f), visually confirming significant anisonucleosis. In contrast, the Compactness distribution remains relatively stable across all categories.

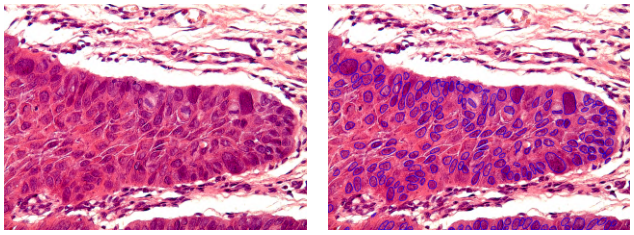

(a) Original H&E Image (b) Segmentation Overlay

Fig. 4. Visualization of the segmentation accuracy. (a) Original H&E micrograph. (b) The same image with the outlines of the Cellpose-segmented nuclei overlaid in color, demonstrating the precise correspondence with the underlying nuclear structures.

from lesions that progressed to cancer versus those that did not, machine learning classifiers can be trained to generate a "malignant transformation risk score". Furthermore, the tool could be expanded to segment other tissue components to build a more comprehensive picture of the tissue microenvironment, which is known to play a role in cancer progression [16].

Another limitation of the current workflow is the non-specific nature of the segmentation algorithm. The method is applied indiscriminately to all cells within the tissue section, without inherent knowledge of diagnostically relevant regions. In the histopathology of OED, the most critical morphological changes are concentrated within the basal and parabasal layers of the epithelium. Consequently, the automated segmentation of nuclei from superficial layers or non-epithelial cells necessitates the significant expert-guided pruning step described in our methods, thereby increasing the reliance on manual intervention.

Future work could address this by incorporating a preliminary tissue compartment classification model. Such a model would first identify the basal and parabasal layers as the region of interest, restricting the subsequent nuclear segmentation and analysis to only the most diagnostically significant cells. This would create a more streamlined and fully automated pipeline, further reducing subjectivity and manual effort.

V. Conclusion

This study successfully demonstrated that a deep learning-based segmentation tool, Cellpose, serves as a precise and effective instrument for the quantitative analysis of nuclear morphology in Oral Epithelial Dysplasia. The tool enables the objective measurement of key dysplastic features, with anisonucleosis emerging as a particularly strong quantitative marker for distinguishing between diagnostic grades and identifying invasive carcinoma. By providing a standardized and reproducible method for extracting morphometric data, this automated approach serves as a promising foundational component for the development of advanced diagnostic and prognostic systems, with the potential to significantly enhance risk stratification for patients with OPMDs.

Acknowledgment

The authors thank the Pontifícia Universidade Católica de Minas Gerais – PUC-Minas, Coordenação de Aperfeiçoamento de Pessoal de Nível Superior – CAPES – (CAPES STIC-AMSUD 88887.878869/2023-00, 23-STIC-10 and Finance Code 001), the Conselho Nacional de Desenvolvimento Científico e Tecnológico – CNPq (Grants 407242/2021-0, 306573/2022-9, 442950/2023-3) and Fundação de Apoio à Pesquisa do Estado de Minas Gerais – FAPEMIG (Grant APQ-01079-23, APQ-05058-23 and PCE-00301-25).

REFERENCES

[1] H. Sung, J. Ferlay, R. L. Siegel, M. Laversanne, I. Soerjomataram, A. Jemal, and F. Bray, "Global cancer statistics 2020: Globocan estimates of incidence and mortality worldwide for 36 cancers in 185 countries," *CA: A Cancer Journal for Clinicians*, vol. 71, no. 3, pp. 209–249, 2021.

[2] S. Warnakulasuriya, "Global epidemiology of oral and oropharyngeal cancer," *Oral Oncology*, vol. 45, no. 4-5, pp. 309–316, 2009.

[3] P. M. Speight, S. A. Khurram, and O. Kujan, "Oral potentially malignant disorders: a practical approach to diagnosis and management," *Journal of Oral Pathology & Medicine*, vol. 47, no. 8, pp. 723–732, 2018.

[4] A. K. El-Naggar, J. K. C. Chan, J. R. Grandis, T. Takata, and P. J. Slootweg, Eds., *WHO Classification of Head and Neck Tumours*, 4th ed., ser. World Health Organization Classification of Tumours. Lyon, France: IARC Press, 2017, vol. 9.

[5] O. Kujan, R. J. Oliver, A. Khattab, S. A. Roberts, N. Thakker, and P. Sloan, "Evaluation of a new binary system of grading oral epithelial dysplasia with correlation to clinical outcome," *Oral Oncology*, vol. 42, no. 10, pp. 987–993, 2006.

[6] D. J. Fischer, J. B. Epstein, T. H. Morton, and S. M. Schwartz, "Interobserver reliability in the histopathologic grading of oral epithelial dysplasia," *Oral Surgery, Oral Medicine, Oral Pathology, Oral Radiology, and Endodontology*, vol. 97, no. 5, pp. 604–610, 2004.

[7] L. M. Abbey, G. E. Kaugars, J. C. Gunsolley, J. C. Burns, D. G. Page, J. A. Svirsky, S. M. Hahn, W. C. Cothran, and C. A. Gendusa, "Interexaminer and intraexaminer reliability in the diagnosis of oral epithelial dysplasia," *Oral Surgery, Oral Medicine, Oral Pathology, Oral Radiology, and Endodontology*, vol. 80, no. 2, pp. 188–191, 1995.

[8] O. Iocca, T. P. Sollecito, F. Alawi, G. S. Weinstein, J. G. Newman, A. De Virgilio, P. Di Maio, G. Spriano, M. Pardiñas, R. M. Shanti, D. C. Lanza, and A. D. Le, "A systematic review of the prognostic significance of the clinical and histopathologic grading of oral epithelial dysplasia," *Oral Surgery, Oral Medicine, Oral Pathology and Oral Radiology*, vol. 113, no. 6, pp. 799–809, 2012.

[9] A. Madabhushi and G. Lee, "Image analysis and machine learning in digital pathology: Challenges and opportunities," *Medical Image Analysis*, vol. 33, pp. 170–175, 2016.

[10] C. Lu, D. Wang, P. Wang, T. Li, and H. Liu, "Nuclear morphometry for grading oral epithelial dysplasia," *Journal of Pathology Informatics*, vol. 7, p. 31, 2016.

[11] C. Stringer, T. Wang, M. Michaelos, and M. Pachitariu, "Cellpose: a generalist algorithm for cellular segmentation," *Nature Methods*, vol. 18, no. 1, pp. 100–106, 2021.

[12] J. P. Vink, J. A. W. M. van der Laak, B. de Hoop, C. A. H.-v. van de Kaa, E. A. Janssen, H. van Boven, and J. Bulten, "A comparison of five different automated and semi-automated nuclear segmentation methods for cervical cytology," *Cytometry Part B: Clinical Cytometry*, vol. 84, no. 5, pp. 322–331, 2013.

[13] T. Rau, E. Horing, N. Stathonikos, M. de Wit, E. Hoving, T. Offermans, M. Trajkovic-Arsic, F. Ciompi, J. van der Laak, and I. D. Nagtegaal, "The application of quantitative image analysis and machine learning in the classification of colorectal polyps," *Modern Pathology*, vol. 34, no. 5, pp. 1010–1020, 2021.

[14] H. R. Tizhoosh and L. Pantanowitz, "Artificial intelligence and digital pathology: challenges and opportunities," *Journal of Pathology Informatics*, vol. 9, p. 38, 2018.

[15] P. Krishnan, R. D. Uthoff, H. An, W. Chen, A. Tanna, T. Tanna, S. Kalmady, H. McGehee, M. Brandwein-Weber, A. K. Lee, R. B. Smith, R. Ganti, and C. Raman, "Quantitative histopathology and nuclear-scale architecture analysis of oral dysplasia," *Scientific Reports*, vol. 9, no. 1, p. 12921, 2019.

[16] R. M. Bremnes, T. Dønnem, S. Al-Saad, K. Al-Shibli, S. Andersen, R. Sirera, C. Camps, and L.-T. Busund, "The role of tumor stroma in cancer progression and therapy: revelation of a new therapeutic target," *Expert Opinion on Therapeutic Targets*, vol. 15, no. 3, pp. 315–325, 2011.